



**HAL**  
open science

## Switching of the magnetic order in $\text{CeRhIn}_5 - x\text{Sn}_x$ in the vicinity of its quantum critical point

S. Raymond, Jonathan Buhot, E. Ressouche, F. Bourdarot, G. Knebel, G.  
Lapertot

► **To cite this version:**

S. Raymond, Jonathan Buhot, E. Ressouche, F. Bourdarot, G. Knebel, et al.. Switching of the magnetic order in  $\text{CeRhIn}_5 - x\text{Sn}_x$  in the vicinity of its quantum critical point. *Physical Review B: Condensed Matter and Materials Physics (1998-2015)*, 2014, 90 (1), 10.1103/PhysRevB.90.014423 . hal-01937756

**HAL Id: hal-01937756**

**<https://hal.science/hal-01937756>**

Submitted on 7 Dec 2018

**HAL** is a multi-disciplinary open access archive for the deposit and dissemination of scientific research documents, whether they are published or not. The documents may come from teaching and research institutions in France or abroad, or from public or private research centers.

L'archive ouverte pluridisciplinaire **HAL**, est destinée au dépôt et à la diffusion de documents scientifiques de niveau recherche, publiés ou non, émanant des établissements d'enseignement et de recherche français ou étrangers, des laboratoires publics ou privés.

## Switching of the magnetic order in $\text{CeRhIn}_{5-x}\text{Sn}_x$ in the vicinity of its quantum critical point

S. Raymond, J. Buhot,\* E. Ressouche, F. Bourdarot, G. Knebel, and G. Lapertot  
*Université Grenoble Alpes, INAC-SPSMS, F-38000 Grenoble, France*  
*and CEA, INAC-SPSMS, F-38000 Grenoble, France*

(Received 16 May 2014; revised manuscript received 2 July 2014; published 18 July 2014)

We report neutron diffraction experiments performed in the tetragonal antiferromagnetic heavy fermion system  $\text{CeRhIn}_{5-x}\text{Sn}_x$  in its  $(x, T)$  phase diagram up to the vicinity of the critical concentration  $x_c \approx 0.40$ , where long range magnetic order is suppressed. The propagation vector of the magnetic structure is found to be  $\mathbf{k}_{\text{IC}} = (1/2, 1/2, k_l)$  with  $k_l$  increasing from  $k_l = 0.298$  to  $k_l = 0.410$  when  $x$  increases from  $x = 0$  to  $x = 0.26$ . Surprisingly, for  $x = 0.30$ , the order has changed drastically and a commensurate antiferromagnetism with  $\mathbf{k}_{\text{C}} = (1/2, 1/2, 0)$  is found. This concentration is located in the proximity of the quantum critical point where superconductivity is expected.

DOI: [10.1103/PhysRevB.90.014423](https://doi.org/10.1103/PhysRevB.90.014423)

PACS number(s): 71.27.+a, 74.70.Tx, 75.25.-j

The interplay between magnetism and superconductivity is one of the most studied topics in the physics of strongly correlated electron systems. The occurrence of competing or coexisting antiferromagnetic and superconducting ground states is common to many systems: high- $T_c$  cuprates, new iron-based superconductors, and heavy fermion (HF) compounds [1]. In this context, the family of HF compounds  $\text{CeMIn}_5$  ( $M = \text{Co}, \text{Rh}, \text{Ir}$ ), the so-called 1-1-5 compounds, is a fabulous playground since the chemical substitution and the application of pressure or magnetic field lead to the possibility to tune the Néel temperature  $T_N$  and the superconducting transition temperature  $T_c$  to different levels with either  $T_N \geq T_c$  or  $T_N \leq T_c$  [2,3]. The parent compound  $\text{CeRhIn}_5$  crystallizes in the tetragonal space group  $P4/mmm$ . It orders magnetically in an incommensurate helicoidal structure below 3.8 K at ambient pressure. Pressure-induced superconductivity occurs above 1 GPa, and at around 2 GPa the Néel temperature equals the superconducting transition temperature. At higher pressure antiferromagnetism is superseded by a pure superconducting state. However, a magnetic field, applied in the basal plane of the tetragonal structure, inside this superconducting phase, restores an antiferromagnetic order. This phase exists even far above the superconducting upper critical field  $H_{c2}$  [4,5]. Such a field-induced antiferromagnetism bears similarity to the one observed in  $\text{CeCoIn}_5$  out of the purely  $d$ -wave superconducting state, although in this latter case the magnetic order disappears at  $H_{c2}$  [6].

Microscopic information on the magnetic structures is essential in order to grasp the different ingredients at play. In  $\text{CeRhIn}_5$ , this is provided essentially by Nuclear Quadrupole Resonance (NQR) [7] since the triple conditions of high magnetic field, high pressure, and low temperature preclude performing neutron diffraction experiments, which were carried out either under pressure [8,9] or under magnetic field [10]. Another possible route is to substitute Sn for In, which acts as a positive pressure in the phase diagram. This substitution corresponds to electron doping. In  $\text{CeRhIn}_{5-x}\text{Sn}_x$ , a quantum critical point occurs for  $x_c \approx 0.40$

[11–13] and pressure-induced superconductivity is reported in  $\text{CeRhIn}_{4.84}\text{Sn}_{0.16}$  above 0.8 GPa with, however, a reduced maximum value of  $T_c$  [14]. In the present work, we determine the evolution of the magnetic structure as a function of  $x$  in  $\text{CeRhIn}_{5-x}\text{Sn}_x$ .

Single crystals of  $\text{CeRhIn}_{5-x}\text{Sn}_x$  were grown by the self-flux method [15] starting with a ratio  $\text{Ce} : \text{Rh} : \text{In} : \text{Sn} = 1 : 1 : 20 : y$ . In Ref. [11], a linear relationship between the actual Sn concentration  $x$  in the crystal and the starting Sn ratio  $y$  in the flux has been found with  $x = 0.4y$ . The same relation in the determination of the actual concentration is used throughout this article since bulk measurements performed on samples of the same batch of the one for the neutron diffraction experiments, for which a preliminary report can be found in Ref. [16], indicate values of  $T_N$  consistent with the study of Bauer *et al.* [11]. No superconductivity is evidenced in these samples at ambient pressure by resistivity or specific-heat measurements. Rectangular-shaped samples were cut for neutron scattering experiment for  $x = 0.10, 0.16, 0.20, 0.26$ , and  $0.30$  with dimensions given in Table I.

The measurements were performed on the two-axis D23-CEA-CRG (Collaborating Research Group) thermal-neutron diffractometer equipped with a lifting detector at the Institut Laue Langevin, Grenoble. A copper monochromator provides an unpolarized beam with a wavelength of  $\lambda = 1.283 \text{ \AA}$ . The samples were mounted in different kinds of cryostats accordingly to their respective Néel temperatures (see Table I). The  $[1, -1, 0]$  direction was set as the vertical axis. For each sample, the crystal structure was refined using several hundred Bragg reflections, and details of the method are given in a previous study performed on  $\text{CeRhIn}_5$  [10]. The additional parameters compared to  $\text{CeRhIn}_5$  are the occupations of the two inequivalent In sites by Sn substituent [In(1) in the Ce plane and In(2) in between these planes]. A previous crystallographic study performed using a neutron four-circle diffractometer on  $x = 0.16$  suggests that Sn preferentially occupies the In(1) site (66%) compared to the In(2) site (34%) [16]. A similar conclusion is drawn from the NQR results obtained for  $x = 0.044$  [17]. In the present study, it is not possible to differentiate between different models of Sn distribution on In sites: they lead to similar least-square factors in the structural refinement and describe the overall Bragg peak intensities equally well. Nevertheless, independently of

\*Present address: Laboratoire Matériaux et Phénomènes Quantiques, UMR 7162 CNRS, Université Paris Diderot, 75205 Paris, France.

TABLE I. Experimental conditions. The sample size is given along the  $a$ -,  $b$ -, and  $c$ -axis directions (in this order). The third column indicates the sample environment used for each measurement. The fourth column gives the total number of measured magnetic Bragg peaks used for the magnetic moment value determination. It is followed after the dash by the number of independent reflections.

$x$	Sample size (mm <sup>3</sup> )	Cryostat	Magnetic peaks
0.10	2×2×1	<sup>4</sup> He	6-4
0.16	2.1×1.3×1.8	<sup>3</sup> He	10-8
0.20	2×2×1	<sup>3</sup> He	9-7
0.26	2×2×2	<sup>3</sup> He and <sup>3</sup> He- <sup>4</sup> He	10-5
0.30	3×3×1	<sup>3</sup> He- <sup>4</sup> He	3-3

the real site occupation knowledge, a reliable scale factor is obtained in view of the normalization of magnetic Bragg peak intensities. Among these different crystallographic models, the occupancy is in the end arbitrarily fixed to the proportion obtained for  $x = 0.16$  and using the actual  $x$  for each sample. The magnetic structures were also determined with the methods exposed in Ref. [10]. Due to the weak signal only a few magnetic Bragg reflections were measured for each  $x$  (see Table I). This necessitates making further assumptions on the magnetic structure that will be described later in the paper. All the structural and magnetic Bragg peaks are resolution limited.

For each concentration, the search for the magnetic propagation vector was made by doing wide scans along  $\mathbf{Q} = (1/2, 1/2, l)$ . In this paper, the scattering vector  $\mathbf{Q}$  is written as  $\mathbf{Q} = \boldsymbol{\tau} + \mathbf{q}$ , where  $\boldsymbol{\tau}$  is a Brillouin zone center and  $\mathbf{q} = (h, k, l)$ . All coordinates are expressed in reciprocal lattice units (r.l.u.). Representative  $\mathbf{Q}$  scans measured for  $x = 0.16$  along  $[0,0,1]$  and  $[1,1,0]$  directions at  $T = 0.4$  K are shown in Fig. 1. Figure 2 shows similar  $\mathbf{Q}$  scans performed along  $[0,0,1]$  with normalized intensities for  $x = 0.10, 0.26$ , and  $0.30$  for temperatures below and above the respective  $T_N$  of each sample. These data show the smooth evolution of the  $c$ -axis component of the propagation vector between  $x = 0.10$  and  $x = 0.26$ . For  $x = 0.30$ , the magnetic peak position becomes commensurate with a zero  $c$ -axis component. It was also checked, for each  $x$ , that a unique propagation vector exists. This is shown in Fig. 2 for  $x = 0.26$ , where no commensurate

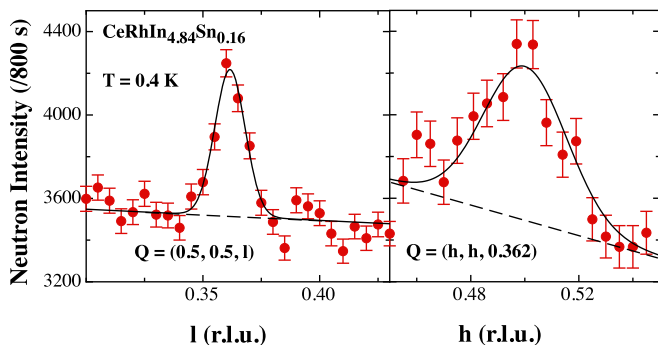


FIG. 1. (Color online)  $\mathbf{Q}$  scans performed along the  $[0,0,1]$  and  $[1,1,0]$  directions for  $\text{CeRhIn}_{4.84}\text{Sn}_{0.16}$  at  $T = 0.4$  K. The full lines are Gaussian fits and the dashed lines indicate the background.

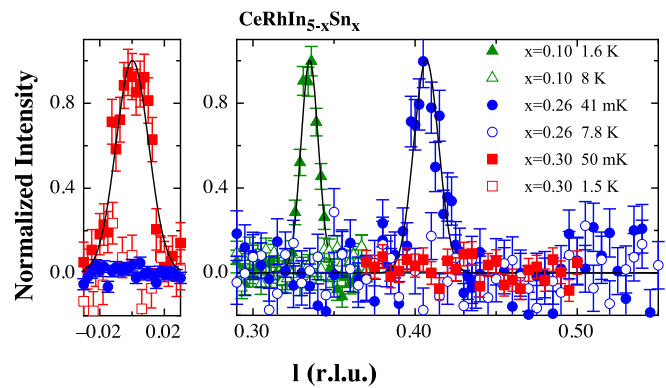


FIG. 2. (Color online)  $\mathbf{Q}$  scans performed along the  $[0,0,1]$  direction for  $x = 0.10, 0.26$ , and  $0.30$  for temperatures below and above their respective Néel temperatures. The full lines are Gaussian fits.

signal is evidenced (full circles) and for  $x = 0.30$  where no incommensurate signal exists (full squares). The main result of this paper is the evidence for a switching of incommensurate magnetic order with  $\mathbf{k}_{\text{IC}} = (1/2, 1/2, k_l)$  ( $0.298 \leq k_l \leq 0.410$ ) to commensurate magnetic order with  $\mathbf{k}_{\text{C}} = (1/2, 1/2, 0)$  (so-called C-type magnetic structure) in  $\text{CeRhIn}_{5-x}\text{Sn}_x$  above  $x = 0.26$ .

Figure 3 shows the temperature dependence of a  $\mathbf{Q}$  scan performed along  $[0,0,1]$  for  $x = 0.20$ . The  $c$ -axis value of the propagation vector,  $k_l$ , does not change significantly with temperature although we cannot exclude a small shift to a lower value in the vicinity of  $T_N$ . The temperature dependence of the order parameter (proportional to the square root of the background subtracted neutron intensity,  $I$ ) was therefore measured on the maximum of the Bragg peak position for each concentration. Normalized intensities ( $I/I_0$ ) are shown in Fig. 4. The Néel temperature given in Table II is obtained from a phenomenological description of these curves with  $I/I_0 \propto 1 - (T/T_N)^\alpha$  with  $\alpha$  a free parameter [18]. The weakness of the signal does not allow us to distinguish between Bragg and diffuse scattering in the vicinity of the phase transition. The best fit is obtained with  $\alpha \approx 6$  for  $x = 0.10, 0.16, 0.20$  and  $\alpha \approx 2$  for  $x = 0.26, 0.30$ . This change of behavior could originate

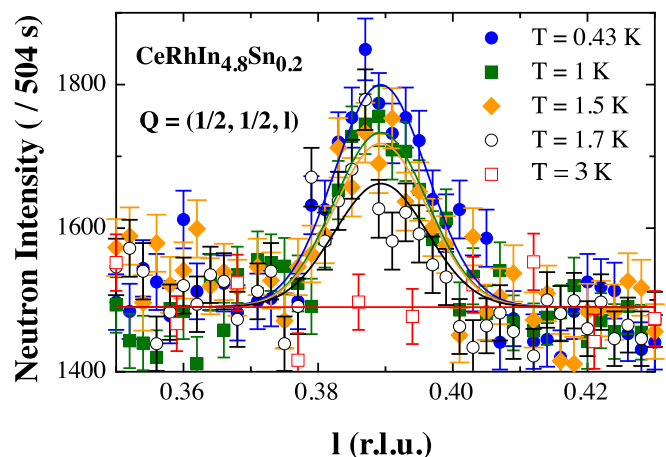


FIG. 3. (Color online) Temperature dependence of a  $\mathbf{Q}$  scan performed along  $[0,0,1]$  for  $x = 0.20$ . Lines are Gaussian fits.

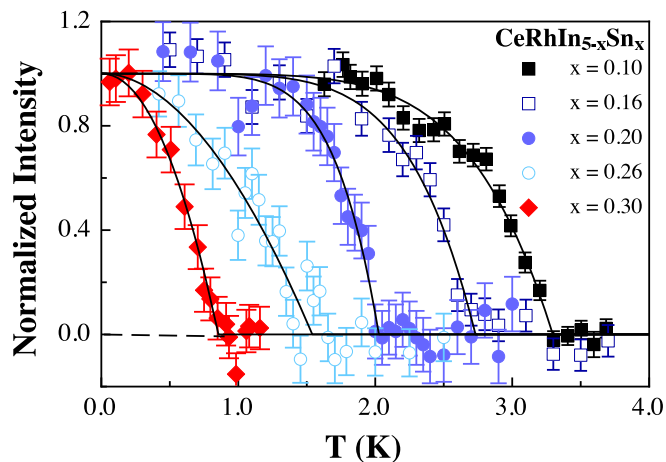


FIG. 4. (Color online) Temperature dependence of the normalized magnetic intensities, for several  $x$ . Lines are phenomenological fits as explained in the text.

from different intrinsic magnetic properties or it could as well be an artifact of this phenomenological method used to determine the Néel temperature. The obtained  $T_N$  values are compatible with the one reported by bulk measurements, keeping in mind that the determinations from specific heat and resistive anomalies show also some differences among themselves [11–14].

For all  $x$ , it is found that, all other factors being taken into account, the magnetic Bragg peak intensities increase when the  $c$ -axis component of  $\mathbf{Q}$  increases. From the magnetic neutron scattering selection rule, this means that the ordered magnetic moments lie mostly in the basal plane of the tetragonal structure. Following this, we assume that the magnetic moment is fully lying in the basal plane of the tetragonal structure [the small number of measured magnetic peaks (Table I) does not allow us to go beyond that point and to discuss the possibility of a small tilt angle of the moment out of the plane]. Similarly to CeRhIn<sub>5</sub> [10], the magnetic moment value was calculated assuming an helicoidal structure rather than a sine-wave structure up to  $x = 0.26$ . This means that the ordered moments are antiferromagnetically coupled in the basal plane and describe a helix of pitch  $2\pi k_l$  along the  $c$  axis. For  $x = 0.30$ , the commensurate propagation vector implies a collinear structure. Consequently for  $x = 0.30$ , two magnetic domains corresponding to two orthogonal in-plane directions of magnetic moments are considered (an equal domain population is assumed). The values of the propagation

TABLE II. Experimental results for the propagation vector  $\mathbf{k}$ , the Néel temperature  $T_N$ , and the ordered moment  $M_0$ .

$x$	$\mathbf{k}$	$T_N$ (K)	$M_0$ ( $\mu_B$ )
0	(0.5, 0.5, 0.298)	3.80 (1)	0.59 (2)
0.10	(0.5, 0.5, 0.335)	3.30 (2)	0.58 (2)
0.16	(0.5, 0.5, 0.362)	2.73 (3)	0.49 (2)
0.20	(0.5, 0.5, 0.389)	2.03 (3)	0.59 (4)
0.26	(0.5, 0.5, 0.410)	1.54 (9)	0.28 (2)
0.30	(0.5, 0.5, 0)	0.84 (3)	0.25 (2)

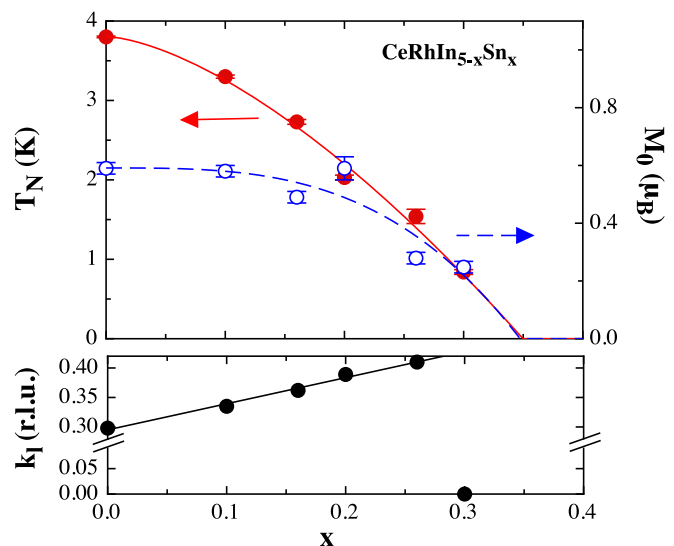


FIG. 5. (Color online) Néel temperature, ordered magnetic moment, and  $c$ -axis component of the propagation vector. Lines are guides for the eyes.

vector  $\mathbf{k}$ , the Néel temperature  $T_N$ , and the ordered moment  $M_0$ , are summarized in Table II and in Fig. 5. The variation of the Néel temperature with  $x$  is smooth and agrees with bulk measurements. The magnetic moment evolves only slightly up to  $x = 0.20$  and then decreases significantly. The  $c$ -axis component of the propagation vector increases linearly with  $x$  up to  $x = 0.26$ , following  $k_l(x) = 0.295(4) + 0.44(2)x$ . For  $x = 0.30$ , the propagation vector has switched to  $\mathbf{k}_C = (1/2, 1/2, 0)$ . The lines drawn for  $T_N(x)$  and  $M_0(x)$  would suggest a critical concentration near 0.35. This is in agreement with the reported value for  $x_c$  that lies between 0.35 [11] and 0.40 [13] depending on whether or not an upturn of  $T_N(x)$  around  $x_c$  is considered.

The main result of this study is the abrupt change of the propagation vector from incommensurate to commensurate in CeRhIn<sub>5-x</sub>Sn<sub>x</sub> in the vicinity of its magnetic quantum critical point where superconductivity is expected to occur. To our knowledge, up to now bulk superconductivity has not been reported at zero pressure for any given  $x$ , but has been observed on applying 0.8 GPa starting from  $x = 0.16$  [14] or 0.6 GPa starting from  $x = 0.20$  [19]. These results suggest that further studies may evidence superconductivity at zero pressure in CeRhIn<sub>5-x</sub>Sn<sub>x</sub> at higher  $x$  near  $x_c$ . On the other hand, when  $x$  increases, disorder increases and this may be detrimental to superconductivity. Having this in mind, one must nonetheless notice that similar changes of magnetic structure are already reported for several 1-1-5 related compounds for which superconductivity is firmly established.

A trend in the generic quantum critical  $(x, P, T)$  phase diagram of CeRhIn<sub>5</sub> related compounds is indeed the change from incommensurate to commensurate ordering associated with the appearance of superconductivity. This is observed for Ir and Co doped CeRhIn<sub>5</sub> for which ordering with  $\mathbf{k}_G = (1/2, 1/2, 1/2)$  (G-type magnetic ordering) is reported either coexisting with or superseding the incommensurate ordering [20–23]. Regarding CeRhIn<sub>5</sub> under pressure, NQR strongly suggests the same G-type commensurate ordering

above 1.7 GPa [7]. This is not confirmed by neutron scattering experiments that were performed up to this pressure. Nonetheless, a switching from  $k_l \approx 0.30$  to  $k_l \approx 0.40$  is found at lower pressure in relation to superconductivity [8,9].

All these data suggest that commensurate antiferromagnetism with  $\mathbf{k}_G = (1/2, 1/2, 1/2)$  is favorable for the formation of superconductivity in the quantum critical phase diagram of CeRhIn<sub>5</sub> related systems. Strikingly, we also observe here a commensurate ordering in CeRhIn<sub>5-x</sub>Sn<sub>x</sub> in the vicinity of  $x_c$  but with  $\mathbf{k}_C = (1/2, 1/2, 0)$  instead of  $\mathbf{k}_G$  that would have been expected. This unachieved expectation was not only built upon the aforementioned literature but also upon the puzzling fact that the extrapolation of  $k_l(x)$  to  $k_l = 1/2$  occurs for  $x \approx x_c$ . In addition, to our knowledge, a C-type magnetic ordering has not been reported yet for rare-earth based 1-1-5 systems. This propagation vector is nonetheless the one of the magnetic order of the actinide based compound NpFeGa<sub>5</sub> [24] and of several rare-earth based compounds related to the 1-1-5 ones by different sequences of atomic stacking [25].

As often pointed out, the Fermi surface topology is likely to play a key role for the determination of the magnetic ordering wave vector. This is specifically demonstrated for CeRhIn<sub>5</sub> by an *ab initio* calculation performed at  $P = 0$  that evidences a nesting of the Fermi surface for  $k_l = 0.375$ , which is very close to the experimental value for the magnetic ordering wave vector  $\mathbf{k}_{IC}$  [26]. de Haas-van Alphen experiments are very powerful for tracking the modification of the Fermi surface as a function of  $P$  or  $x$ . A change of Fermi surface from localized character to itinerant character occurs under pressure in CeRhIn<sub>5</sub> at around 2.3 GPa where the superconducting transition temperature is maximum [27]. In a different way, Fermi surface reconstruction is also reported for Co substituted CeRhIn<sub>5</sub> when the magnetic structure switches from incommensurate to commensurate antiferromagnetism and when superconductivity occurs [28]. We can speculate that an abrupt modification of the Fermi surface occurs in CeRhIn<sub>5-x</sub>Sn<sub>x</sub>

between  $x = 0.26$  and  $x = 0.30$  and this drives the switching of the propagation vector.

The systems reviewed above realize a case where  $T_N$  is higher than  $T_c$  and incommensurate magnetic ordering with  $\mathbf{k}_{IC} = (1/2, 1/2, k_l)$  seems to be detrimental to superconductivity. The opposite situation ( $T_N \leq T_c$ ) is also of great interest although experimental realization are scarce. Recently we have shown that in Ce<sub>0.95</sub>Nd<sub>0.05</sub>CoIn<sub>5</sub> magnetic ordering with the incommensurate propagation vector  $\mathbf{k}_Q = (0.45, 0.45, 0.5)$  occurs [29]. This is the same propagation vector as the one of the field-induced antiferromagnetic phase of CeCoIn<sub>5</sub> starting from the pure *d*-wave superconducting state. Here again Fermi surface topology is believed to play a key role. Since in both cases magnetic ordering occurs when superconductivity is established, it was suggested that *d*-wave superconductivity with nodes in the nesting area favors such an incommensurate order with in-plane incommensurability.

Altogether these results suggest the possibility of collaborative effects between magnetism and superconductivity in the family of 1-1-5 compounds in relation to fine details of the Fermi surface. While the involved mechanisms are not necessarily the same for all these systems, magnetism and superconductivity can either compete or collaborate in 1-1-5 systems. These two opposite situations are likely to originate from the position of the nesting vector on the Fermi surface with respect to the superconducting order parameter nodes' position.

In summary, we evidence a switching of magnetic propagation vector from incommensurate with  $\mathbf{k}_{IC} = (1/2, 1/2, k_l)$  to commensurate with  $\mathbf{k}_C = (1/2, 1/2, 0)$  in CeRhIn<sub>5-x</sub>Sn<sub>x</sub> in the proximity of its quantum critical point. Taking with caution the  $P$ - $x$  analogy, this would correspond to a region of the phase diagram where superconductivity arises.

We acknowledge K. Mony for help in sample preparation. Cerium was provided by the Materials Preparation Center, Ames Laboratory, US DOE Basic Energy Sciences, Ames, IA, USA, available from [www.mpc.ameslab.gov](http://www.mpc.ameslab.gov).

- 
- [1] Y. Uemura, *Nat. Mater.* **8**, 253 (2009).  
 [2] J. L. Sarrao and J. D. Thompson, *J. Phys. Soc. Jpn.* **76**, 051013 (2007), and references therein.  
 [3] G. Knebel, D. Aoki, and J. Flouquet, *C. R. Physique* **12**, 542 (2011), and references therein.  
 [4] G. Knebel, D. Aoki, D. Braithwaite, B. Salce, and J. Flouquet, *Phys. Rev. B* **74**, 020501 (2006).  
 [5] T. Park, F. Ronning, H. Q. Yuan, M. B. Salamon, R. Movshovich, J. L. Sarrao, and J. D. Thompson, *Nature (London)* **440**, 65 (2006).  
 [6] M. Kenzelmann, Th. Strässle, C. Niedermayer, M. Sigrist, B. Padmanabhan, M. Zolliker, A. D. Bianchi, R. Movshovich, E. D. Bauer, J. L. Sarrao, and J. D. Thompson, *Science* **321**, 1652 (2008), and references therein.  
 [7] M. Yashima, H. Mukuda, Y. Kitaoka, H. Shishido, R. Settai, and Y. Onuki, *Phys. Rev. B* **79**, 214528 (2009), and references therein.  
 [8] S. Raymond, G. Knebel, D. Aoki, and J. Flouquet, *Phys. Rev. B* **77**, 172502 (2008).  
 [9] N. Aso, K. Ishii, H. Yoshizawa, T. Fujiwara, Y. Uwatoko, G.-F. Chen, N. K. Sato, and K. Miyake, *J. Phys. Soc. Jpn.* **78**, 073703 (2009).  
 [10] S. Raymond, E. Ressouche, G. Knebel, D. Aoki, and J. Flouquet, *J. Phys.: Condens. Matter* **19**, 242204 (2007).  
 [11] E. Bauer, D. Mixson, F. Ronning, N. Hur, R. Movshovich, J. Thompson, J. Sarrao, M. Hundley, P. Tobash, and S. Bobev, *Physica B* **378–380**, 142 (2006).  
 [12] J. G. Donath, F. Steglich, E. D. Bauer, F. Ronning, J. L. Sarrao, and P. Gegenwart, *Europhys. Lett.* **87**, 57011 (2009).  
 [13] J. G. Donath, P. Gegenwart, F. Steglich, E. D. Bauer, and J. L. Sarrao, *Physica C* **460–462**, 661 (2007).  
 [14] L. Mendonça Ferreira, T. Park, V. Sidorov, M. Nicklas, E. M. Bittar, R. Lora-Serrano, E. N. Hering, S. M. Ramos, M. B. Fontes, E. Baggio-Saitovich, H. Lee, J. L. Sarrao, J. D. Thompson, and P. G. Pagliuso, *Phys. Rev. Lett.* **101**, 017005 (2008).  
 [15] P. C. Canfield and Z. Fisk, *Philos. Mag. B* **65**, 1117 (1992).

- [16] G. Knebel, J. Buhot, D. Aoki, G. Lapertot, S. Raymond, E. Ressouche, and J. Flouquet, *J. Phys. Soc. Jpn.* **80**, SA001 (2011).
- [17] J. Ruzs, P. M. Oppeneer, N. J. Curro, R. R. Urbano, B.-L. Young, S. Lebegue, P. G. Pagliuso, L. D. Pham, E. D. Bauer, J. L. Sarrao, and Z. Fisk, *Phys. Rev. B* **77**, 245124 (2008).
- [18] N. Kernavanois, S. Raymond, E. Ressouche, B. Grenier, J. Flouquet, and P. Lejay, *Phys. Rev. B* **71**, 064404 (2005), and reference therein.
- [19] G. Knebel (unpublished).
- [20] A. Llobet, A. D. Christianson, W. Bao, J. S. Gardner, I. P. Swainson, J. W. Lynn, J.-M. Mignot, K. Prokes, P. G. Pagliuso, N. O. Moreno, J. L. Sarrao, J. D. Thompson, and A. H. Lacerda, *Phys. Rev. Lett.* **95**, 217002 (2005).
- [21] S. Ohira-Kawamura, H. Shishido, A. Yoshida, R. Okazaki, H. Kawano-Furukawa, T. Shibauchi, H. Harima, and Y. Matsuda, *Phys. Rev. B* **76**, 132507 (2007).
- [22] M. Yokoyama, N. Oyama, H. Amitsuka, S. Oinuma, I. Kawasaki, K. Tenya, M. Matsuura, K. Hirota, and T. J. Sato, *Phys. Rev. B* **77**, 224501 (2008).
- [23] S. Ohira-Kawamura, H. Kawano-Furukawa, H. Shishido, R. Okazaki, T. Shibauchi, H. Harima, and Y. Matsuda, *Phys. Status Solidi A* **206**, 1076 (2009).
- [24] F. Honda, N. Metoki, K. Kaneko, D. Aoki, Y. Homma, E. Yamamoto, Y. Shiokawa, Y. Onuki, E. Colineau, N. Bernhoeft, and G. Lander, *Physica B* **359-361**, 1147 (2005).
- [25] P. Čermák, P. Javorský, M. Kratochvílová, K. Pajskr, M. Klicpera, B. Ouladdiaf, M.-H. Lemée-Cailleau, J. Rodriguez-Carvajal, and M. Boehm, *Phys. Rev. B* **89**, 184409 (2014), and references therein.
- [26] T. Bjorkman, R. Lizarraga, F. Bultmark, O. Eriksson, J. M. Wills, A. Bergman, P. H. Andersson, and L. Nordstrom, *Phys. Rev. B* **81**, 094433 (2010).
- [27] H. Shishido, R. Settai, H. Harima, and Y. Onuki, *J. Phys. Soc. Jpn.* **74**, 1103 (2005).
- [28] S. K. Goh, J. Paglione, M. Sutherland, E. C. T. O'Farrell, C. Bergemann, T. A. Sayles, and M. B. Maple, *Phys. Rev. Lett.* **101**, 056402 (2008).
- [29] S. Raymond, S. M. Ramos, D. Aoki, G. Knebel, V. P. Mineev, and G. Lapertot, *J. Phys. Soc. Jpn.* **83**, 013707 (2014).